LLNL-TR-409098

LAWRENCE
LIVERMORE
NATIONAL
LABORATORY

# ODS Characterization Progress Report 06/27/08

B. El-Dasher

December 1, 2008

This work performed under the auspices of the U.S. Department of Energy by Lawrence Livermore National Laboratory under Contract DE-AC52-07NA27344.

# ODS Characterization Progress Report 06/27/08

Bassem El-Dasher

## *Introduction*

This progress report is intended to help keep track of the work that has been performed in characterizing ODS steels for the LIFE project. This specific report details the current status of the characterization of a 24% Cr, 1% $Y_2O_3$ ODS steel obtained from Wayne King via Geoff Campbell. Since no pedigree of the material could be obtained, a baseline characterization was necessary prior to studying processing, welding, and corrosion behavior.

This document details the results obtained from analysis performed using scanning electron microscopy (SEM), electron backscatter diffraction (EBSD) and energy dispersive spectroscopy (EDS). At the time of writing, transmission electron microscopy (TEM) and microhardness measurements have not been completed, and will be included in a future report.

## *Results*

The results are presented in two sections: microstructure, and phase identification. As the names suggest, the first section will report on the microstructure in the general sense and include details such as grain size and texture, and the second section will include the identification of the phases present in the baseline material.

*Baseline Microstructure:*

The material in its as-received condition was a hot extruded rod of 5/8" diameter of ODS steel encased in a stainless steel outer cladding. Both cross and longitudinal section (Fig. 1) specimens were prepared for metallographic examination. EBSD scans were performed in order to determine grain size and morphology (Fig. 2). As is typical in an extruded metal, elongated grains were observed. The average diameter of the grains in the cross section was

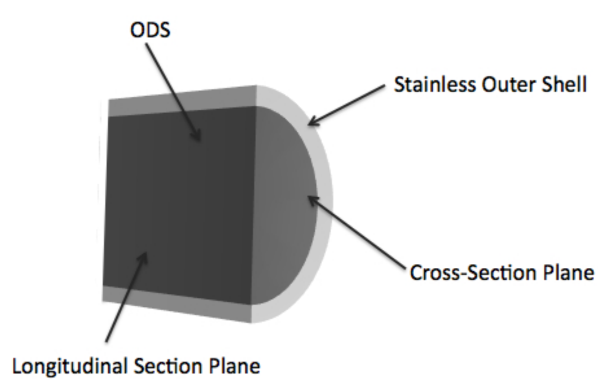


**Figure 1. Schematic of as-received material illustrating examined sections.**

approximately 0.4μm, while the average length of the grains in the longitudinal section (parallel to the extrusion direction) was ~1μm. As can be seen in Fig. 2 some grains in the longitudinal section were significantly longer (over 6μm).

The texture of the material was also calculated from the orientation information obtained from the EBSD scans. The pole figure set in Fig. 3(a) clearly shows a strong (110) texture along the extrusion direction, typical of directionally deformed bcc materials. More importantly, the texture in the cross sectional plane is significantly weaker (around the circumference of the pole figures), which is verified by examining the pole figures from the longitudinal section in Fig. 3 (b), which only show a very weak (111) texture. The significance of this is that we can examine the corrosion behavior of both types of samples (textured and non-textured) by selecting the sections exposed during future corrosion tests to determine if texture should be a consideration when creating the material specification.

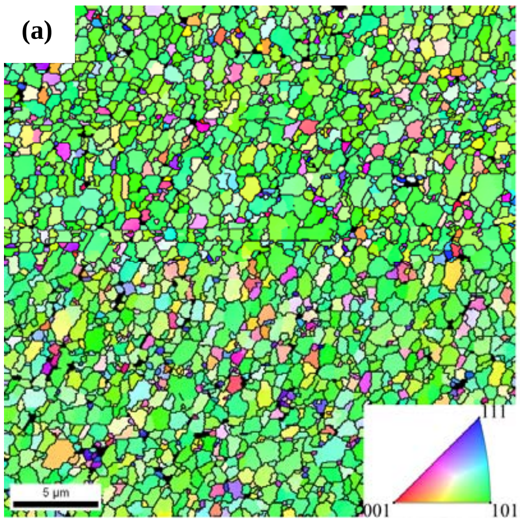


**Figure 2. Electron backscatter inverse pole figure maps for the cross section (a) and longitudinal section (b). Colors correspond to crystal axes parallel to surface normal given in the color-keyed standard stereographic triangle.**

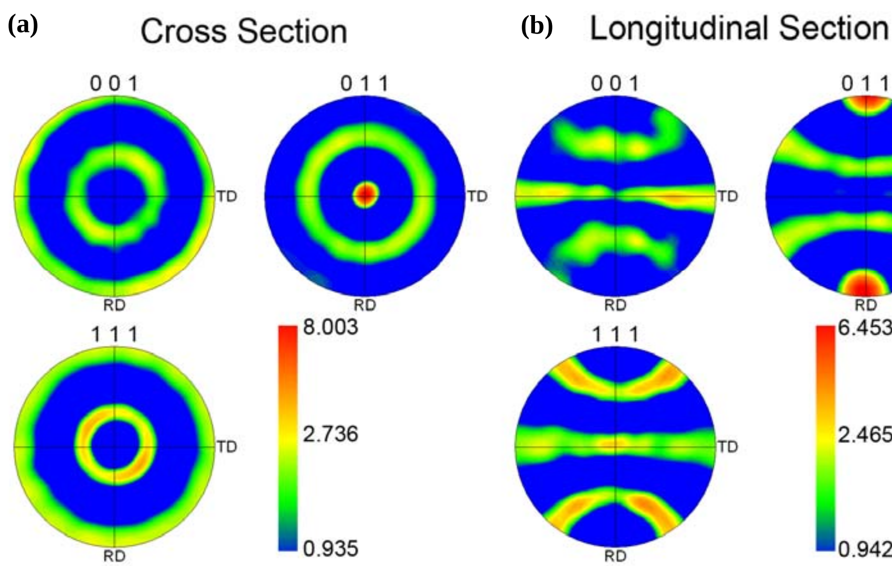


**Figure 3. (001), (011), and (111) pole figures calculated from EBSD scans from both (a) cross and (b) longitudinal sections. A strong (011) texture can be observed along the extrusion direction, while a weak (111) texture orthogonal to the extrusion direction.**

*Phase Identification:*

During the course of preparing for the EBSD scans, it was easily observable in the SEM that secondary phase particles were present. These were prevalent throughout the microstructure, as shown in Fig. 4. Intuitively it was known that these could not be yttria agglomerates, as the amount present was significantly more than 1% (area fraction measurements indicated ~8% secondary phase content). The initial assumption was that perhaps these were σ precipitates that formed during the hot extrusion, as an examination of the Fe-Cr phase diagram (Fig. 5) shows this phase to be stable for the alloy's composition.

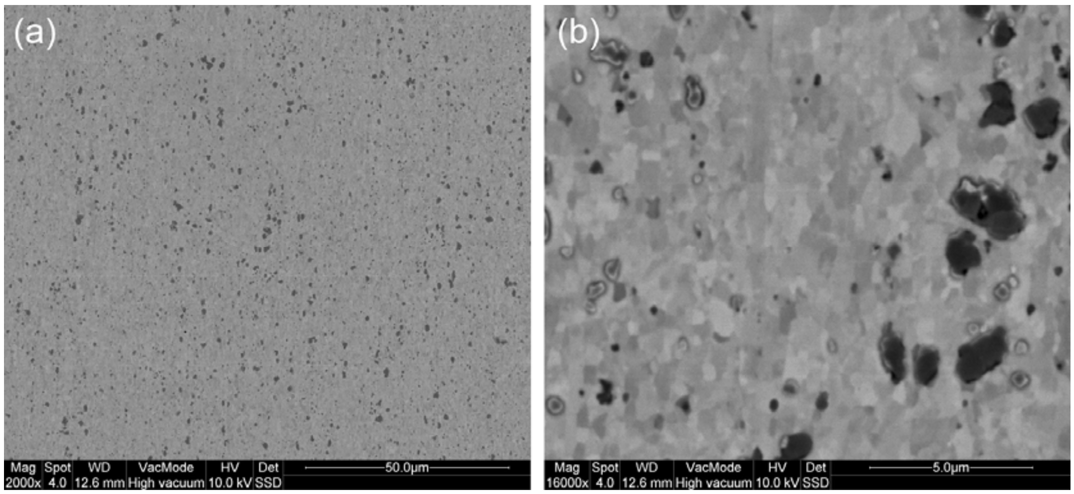


**Figure 4. Backscattered electron micrographs recorded at (a) 2000x and (b) 16000x. Lighter shaded regions are the bcc matrix, and the dark shaded regions are secondary phases.**

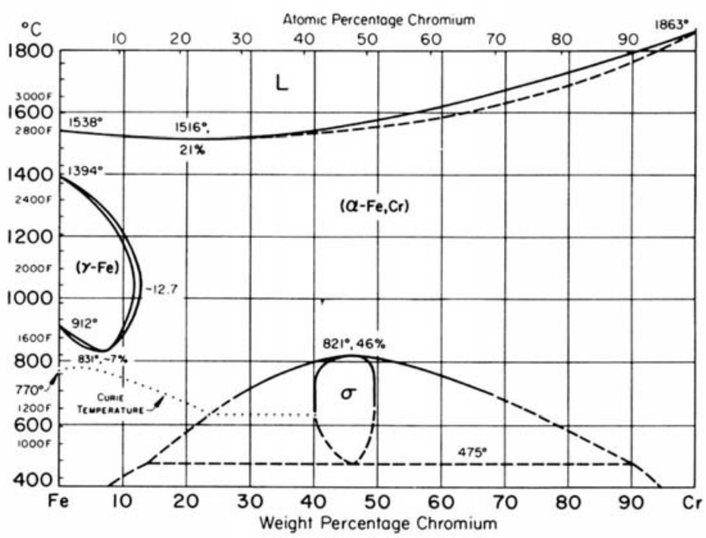


**Figure 5. Iron-Chromium binary phase diagram showing the stability of the σ phase below 700°C for 24% Cr. (Source: George Krauss, Steels: Processing, Structure, and Performance, Fifth Edition,ASM International, 2005, p 496).**

EDS scans however showed these particles to yield a very small iron signature and a high oxygen signature (Fig. 6). A “weaker” electron beam was used (10kV accelerating voltage and the smallest spot size) to obtain an energy spectrum solely from the near surface material, and focusing this beam on one of the particles revealed that no iron was present (Fig. 7).

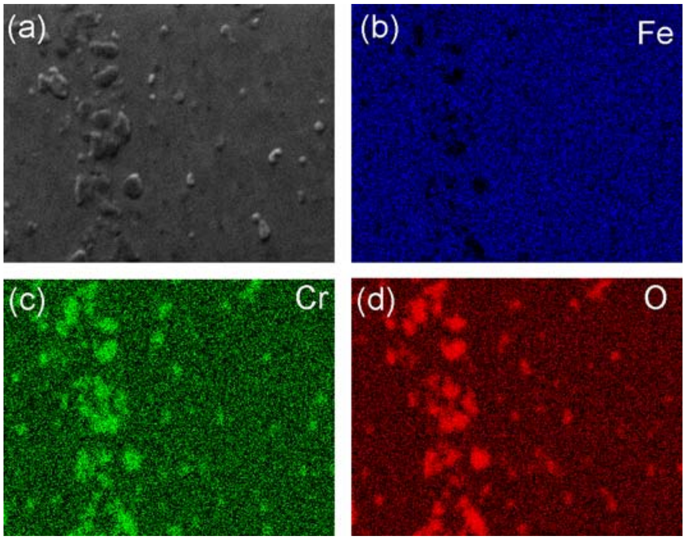


**Figure 6.** EDS area maps showing the secondary electron image (a), distribution of iron (b), chromium (c), and oxygen (d). The secondary particles are observed to be enriched in Cr and O, and deficient in O.

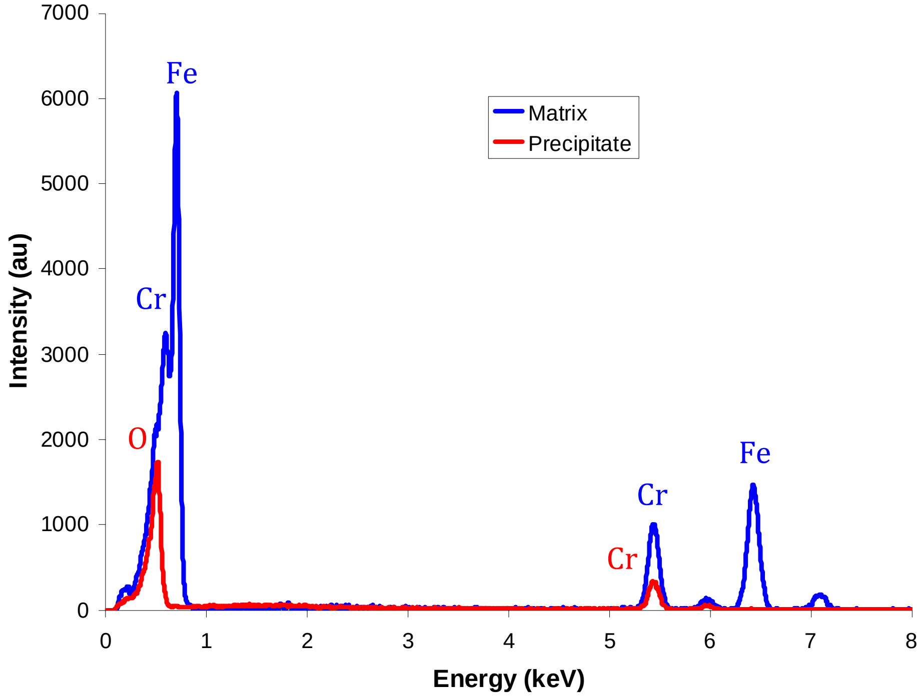


**Figure 7.** EDS spectrum obtained from both the matrix (in blue), and a single secondary phase particle (in red). Note the lack of iron signal in spectrum obtained from the secondary phase.

The stoichiometry was that of $Cr_2O_3$, and diffraction patterns obtained using EBSD form individual particles were used to confirm this. Since the crystal structure of $Cr_2O_3$ is known (corundum, Fig. 8(a)), a material file with the appropriate crystallographic parameters was generated and used to index the diffraction patterns. Using this, indexing of the secondary phase patterns was easily achieved (e.g. Fig. 8(b)), and simulated diffraction patterns were used for visual confirmation (Fig. 8(c)). These results have been corroborated using XRD, not shown since further analysis of the XRD results is necessary, and will be presented in a future summary report.

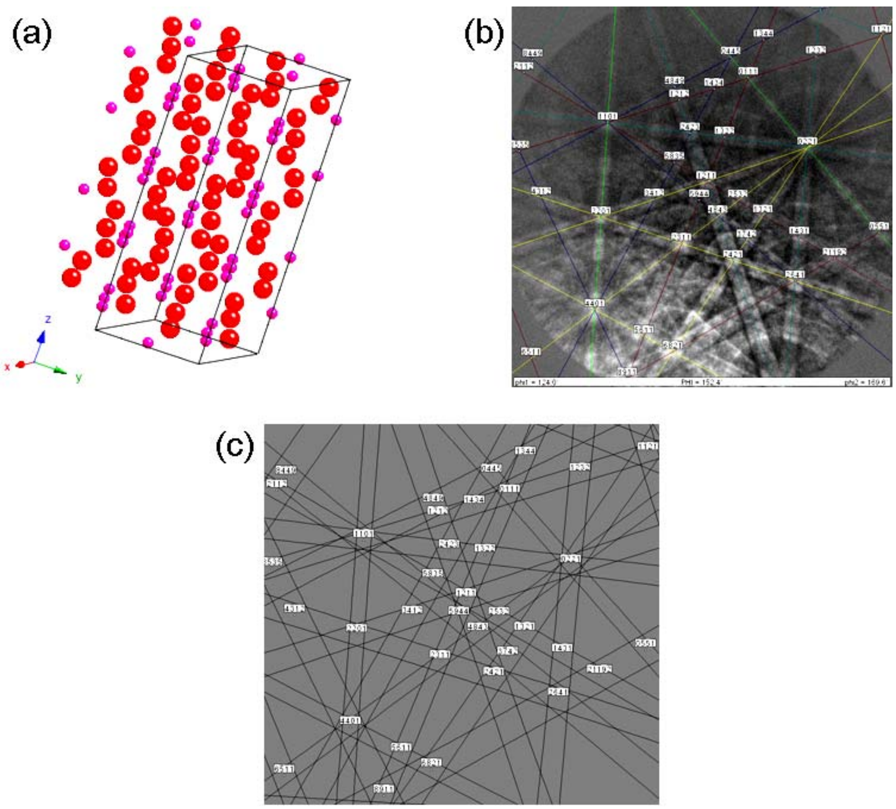

**Figure 8. Determination of secondary phase using electron diffraction. Using the crystallography of $Cr_2O_3$, hexagonal cell shown in (a), captured diffraction patterns were indexed (b), and confirmed by comparison to simulated diffraction pattern (c).**

## *Conclusions*

The ODS steel characterized in this work consists of elongated fine grains (<1μm diameter) that are highly textured along the extrusion axis. Despite the high chromium content, no σ phase was found, but instead a significant amount (~8%) of $Cr_2O_3$ was found. This raises a concern about the weldability, corrosion performance, and mechanical behavior of this specific alloy, as these oxides will strengthen the material further in addition to the yttria.

While we should attempt to purchase or fabricate an ODS steel with a lower chromium content to minimize the presence of this oxide, continuing this study on this material will be quite useful. Besides the fact that this is the only ODS composition in our possession (which allows us to move forward by establishing experimental techniques and devise tests), continuing this study will provide invaluable information for determining the material's performance as a function of the alloy composition.